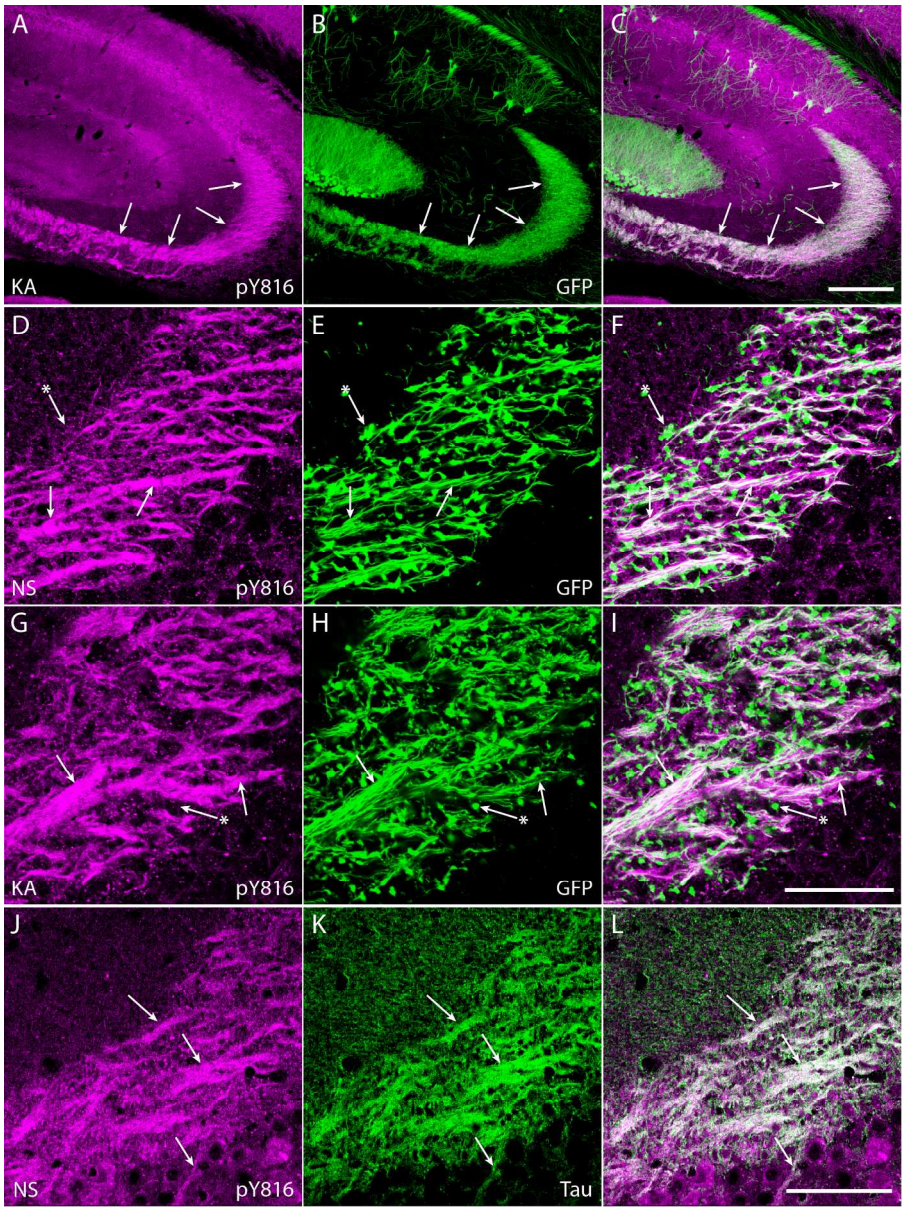

Supplementary Figure 1. pY816 TrkB immunoreactivity colocalizes with axons of dentate granule cells (DGCs) in SL of hippocampus under both NS conditions and following KA-SE. A-C) Images of CA3 region of hippocampus from a KA treated animal demonstrates striking overlap of enhanced pY816 immunoreactivity (A; arrows) with GFP-labeled mossy fibers (B; arrows) that populate SL. Merged pY816 and GFP is shown in (C). Scale bar = 200 µm. D-I) Images from CA3b of SL of sections stained with pY816 (D, G) that also contain GFP (E, H) under conditions of NS infusion (D-F) and following KA-SE (G-I). A subset of mossy fiber axons of DGCs (E, H; arrows) are filled with GFP, and can be seen to colocalize with pY816 (D, G; arrows) under both NS and KA conditions. In contrast, most mossy fiber boutons (E, H; arrows with asterisks) do not contain prominent pY816 immunoreactivity (D, G; arrows with asterisks) compared to axons. Note that the distribution of immunoreactivity does not change between NS and KA treated animals. Merged pY816 and GFP is shown in (F, I). Scale bar = 50 µm. J-L) Images from CA3b of SL from a control animal stained with pY816 (J) and tau (K), an axonal protein. Tau stained mossy fiber axon tracts (K; arrows) prominently colocalize with pY816 (J; arrows). Merged pY816 and Tau is shown in (L). Scale bar = 50 µm.

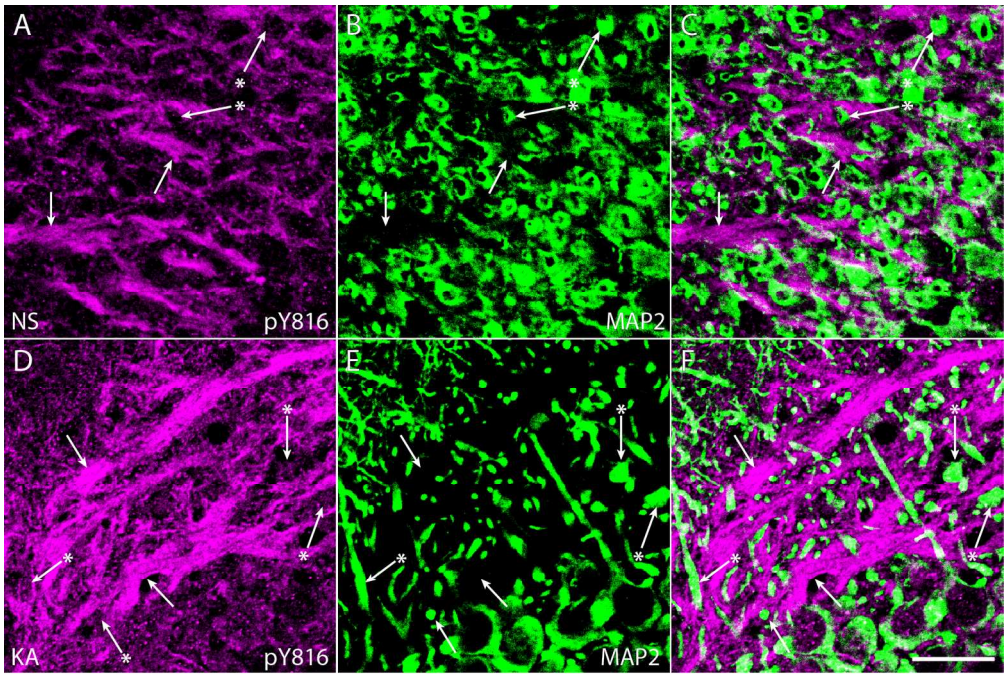

Supplementary Figure 2. pY816 TrkB immunoreactivity does not prominently colocalize with MAP2 stained dendrites of CA3 pyramids under either NS conditions or following KA-SE. A-F) Images from CA3b of SL of pY816 stained sections (A, D) co-stained with MAP2 (B, E), a marker of dendrites, under conditions of NS infusion (A-C) and following KA-SE (D-F). Linear patches of pY816 immunoreactivity (A, D; arrows), demonstrated to colocalize with mossy fiber axons (Fig. 3 and Supplementary Fig. 1), do not colocalize with MAP2 (B, E; arrows). Furthermore, MAP2 labeled dendrites of CA3 pyramidal cells (B, E; arrows with asterisks) do not contain prominent pY816 immunoreactivity (A, D; arrows with asterisks). Merged pY816 and MAP2 is shown in (C, F). No apparent differences are observed in the cellular distributions of pY816 immunoreactivity between NS and KA treated animals. Scale bar = 20 μm.
172x114mm (300 x 300 DPI)

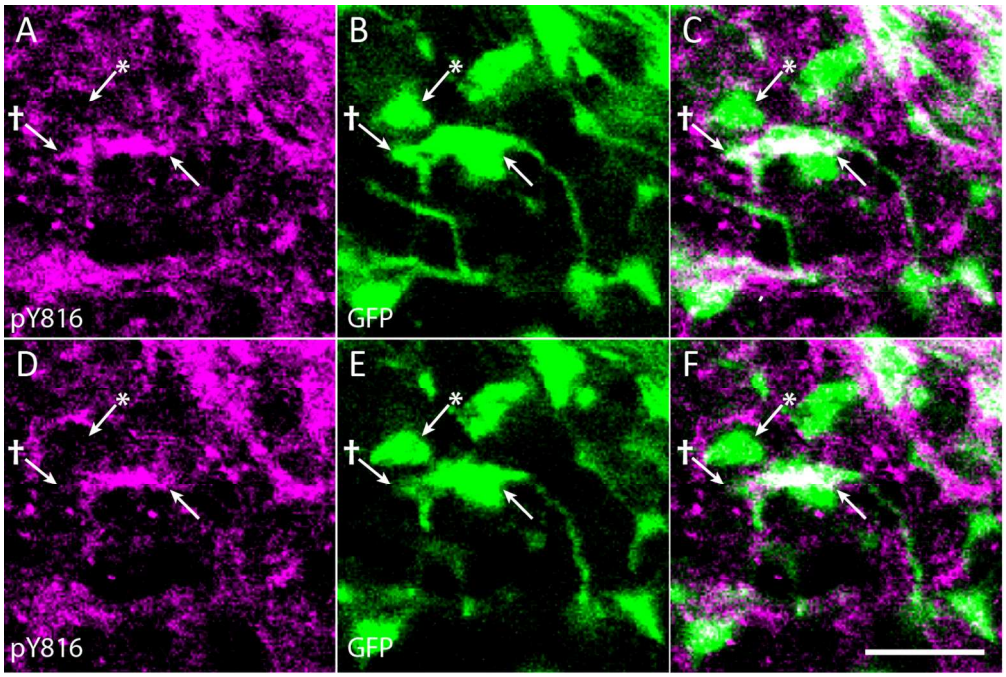

Supplementary Figure 3. pY816 TrkB immunoreactivity is enhanced within synaptic mossy fiber boutons in SL following KA-SE, observed preferentially in the hippocampus ipsilateral to infusion. A-F) Confocal micrographs of two z-sections (A-D, z-section one; D-F, z-section two) taken at a 1 µm increment containing GFP+ mossy fiber boutons (B, E; arrow and arrow with asterisk) within SL ipsilateral to infusion in a KA treated animal. One bouton contains obvious pY816 immunoreactivity (A, D; arrow), whereas an adjacent bouton does not contain prominent pY816 (A, D; arrow with asterisk). Merged pY816 and GFP is shown in (C, F). A pY816 puncta within the bouton (A-C; arrow with dagger) disappears as the portion of the bouton containing it leaves the focal plane (D-F; arrow with dagger). Scale bar = 3.3 µm.
127x85mm (300 x 300 DPI)

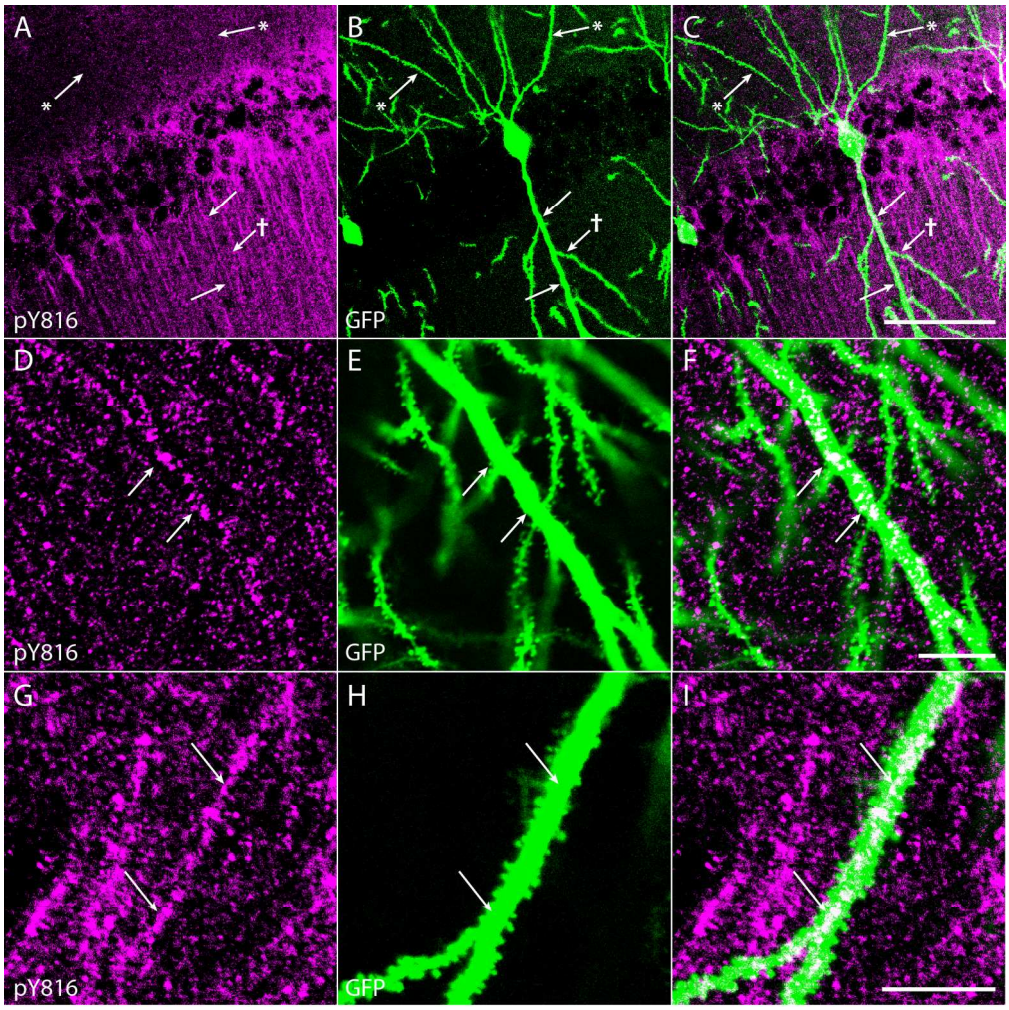

Supplementary Figure 4. pY816 TrkB immunoreactivity is intracellular and punctate within the dendritic shaft of proximal apical dendrites of CA1 pyramidal cells. A-C) The primary apical dendrite of a GFP+ CA1 pyramidal neuron (B; arrows) contains clear pY816 immunoreactivity (A; arrows) within its aspinous proximal shaft, whereas a secondary dendritic branch (B; arrow with dagger) does not contain prominent immunoreactivity within its shaft (A; arrow with dagger). Basal dendritic processes (B; arrows with asterisks) clearly do not contain pY816 immunoreactivity (A; arrows with asterisks). Merged pY816 and GFP is shown in (C). Image is a maximum projection (displaying the region of highest intensity) of multiple confocal scans taken at 0.4 µm increments in the z-plane. Scale bar = 50 µm. D-F) Close-up of a proximal, aspinous portion of a GFP+ apical dendritic process (E; arrows) with intracellular, punctate pY816 immunoreactivity (D; arrows) within the shaft. Merged pY816 and GFP is shown in (F). Scale bar = 10 µm. G-I) A spiny portion of a GFP+ apical dendrite (H; arrows) also displaying intracellular, punctate pY816 immunoreactivity (G; arrows) within the shaft. Merged pY816 and GFP is shown in (I). Scale bar = 10 µm.
172x172mm (300 x 300 DPI)

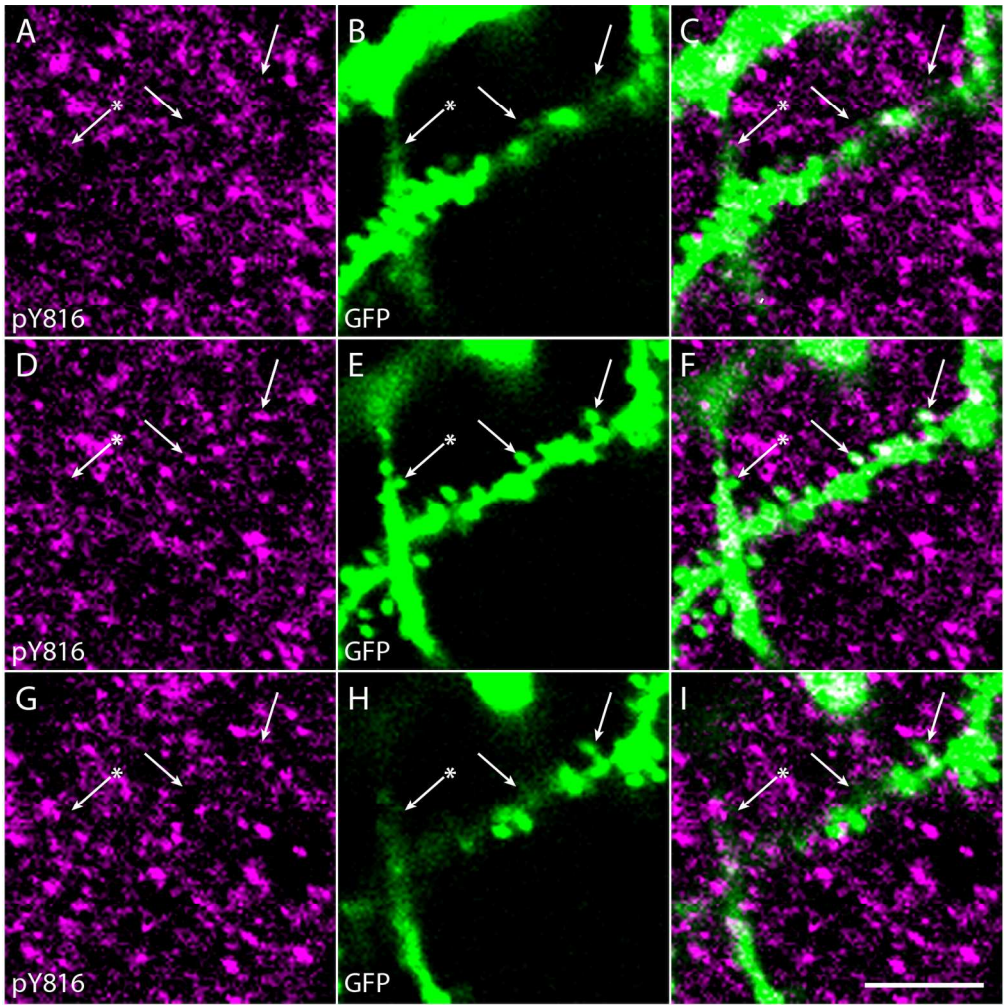

Supplementary Figure 5. pY816 TrkB immunoreactivity is enhanced within dendritic spines in CA1 SR following KA-SE, observed preferentially in the hippocampus ipsilateral to infusion. A-I) Confocal micrographs from CA1 SR from a Thy1-GFP mouse treated with KA. Three z-sections are shown taken at 750 nm increments above (A-C; top), within (D-F; middle), and below (G-I; bottom) two GFP+ spines (E; arrows) of an apical dendrite that contain small pY816 puncta (D; arrows). Other spines (E; arrow with asterisk) do not appear to contain pY816 (D; arrow with asterisk). Note colocalization of pY816 with spines in the z-plane (observe panels from top to bottom and note arrows), such that these pY816 puncta are observable within the spine but not above or below it. Merged pY816 and GFP images are shown in (C, F, I). Scale bar = 2.5 µm.
152x152mm (300 x 300 DPI)

Supplementary Figure 1: (magenta-green version of Figure 3 for the assistance of color-blind readers. pY816 TrkB immunoreactivity colocalizes with axons of dentate granule cells (DGCs) in SL of hippocampus under both NS conditions and following KA-SE. A-C) Images of CA3 region of hippocampus from a KA treated animal demonstrates striking overlap of enhanced pY816 immunoreactivity (A; arrows) with GFP-labeled mossy fibers (B; arrows) that populate SL. Merged pY816 and GFP is shown in (C). Scale bar = 200 μm. D-I) Images from CA3b of SL of sections stained with pY816 (D, G) that also contain GFP (E, H) under conditions of NS infusion (D-F) and following KA-SE (G-I). A subset of mossy fiber axons of DGCs (E, H; arrows) are filled with GFP, and can be seen to colocalize with pY816 (D, G; arrows) under both NS and KA conditions. In contrast, most mossy fiber boutons (E, H; arrows with asterisks) do not contain prominent pY816 immunoreactivity (D, G; arrows with asterisks) compared to axons. Note that the distribution of immunoreactivity does not change between NS and KA treated animals. Merged pY816 and GFP is shown in (F, I). Scale bar = 50 μm. J-L) Images from CA3b of SL from a control animal stained with pY816 (J) and tau (K), an axonal protein. Tau stained mossy fiber axon tracts (K; arrows) prominently colocalize with pY816 (J; arrows). Merged pY816 and Tau is shown in (L). Scale bar = 50 μm.

Supplementary Figure 2: (magenta-green version of Figure 4 for the assistance of color blind readers. pY816 TrkB immunoreactivity does not prominently colocalize with MAP2 stained dendrites of CA3 pyramids under either NS conditions or following KA-SE.) A-F) Images from CA3b of SL of pY816 stained sections (A, D) co-stained with MAP2 (B, E), a marker of dendrites, under conditions of NS infusion (A-C) and following

KA-SE (D-F). Linear patches of pY816 immunoreactivity (A, D; arrows), demonstrated to colocalize with mossy fiber axons (Fig. 3 and Supplementary Fig. 1), do not colocalize with MAP2 (B, E; arrows). Furthermore, MAP2 labeled dendrites of CA3 pyramidal cells (B, E; arrows with asterisks) do not contain prominent pY816 immunoreactivity (A, D; arrows with asterisks). Merged pY816 and MAP2 is shown in (C, F). No apparent differences are observed in the cellular distributions of pY816 immunoreactivity between NS and KA treated animals. Scale bar = 20 μm.

Supplementary Figure 3: (magenta-green version of Figure 5 for the assistance of color-blind readers. pY816 TrkB immunoreactivity is enhanced within synaptic mossy fiber boutons in SL following KA-SE, observed preferentially in the hippocampus ipsilateral to infusion.) A-F) Confocal micrographs of two *z*-sections (A-D, *z*-section one; D-F, *z*-section two) taken at a 1 μm increment containing GFP+ mossy fiber boutons (B, E; arrow and arrow with asterisk) within SL ipsilateral to infusion in a KA treated animal. One bouton contains obvious pY816 immunoreactivity (A, D; arrow), whereas an adjacent bouton does not contain prominent pY816 (A, D; arrow with asterisk). Merged pY816 and GFP is shown in (C, F). A pY816 puncta within the bouton (A-C; arrow with dagger) disappears as the portion of the bouton containing it leaves the focal plane (D-F; arrow with dagger). Scale bar = 3.3 μm.

Supplementary Figure 4: (magenta-green version of Figure 7 for the assistance of color-blind readers. pY816 TrkB immunoreactivity is intracellular and punctate within the dendritic shaft of proximal apical dendrites of CA1 pyramidal cells.) A-C) The primary apical dendrite of a GFP+ CA1 pyramidal neuron (B; arrows) contains clear pY816 immunoreactivity (A; arrows) within its aspinous proximal shaft, whereas a

secondary dendritic branch (B; arrow with dagger) does not contain prominent immunoreactivity within its shaft (A; arrow with dagger). Basal dendritic processes (B; arrows with asterisks) clearly do not contain pY816 immunoreactivity (A; arrows with asterisks). Merged pY816 and GFP is shown in (C). Image is a maximum projection (displaying the region of highest intensity) of multiple confocal scans taken at 0.4 μm increments in the *z*-plane. Scale bar = 50 μm. D-F) Close-up of a proximal, aspinous portion of a GFP+ apical dendritic process (E; arrows) with intracellular, punctate pY816 immunoreactivity (D; arrows) within the shaft. Merged pY816 and GFP is shown in (F). Scale bar = 10 μm. G-I) A spiny portion of a GFP+ apical dendrite (H; arrows) also displaying intracellular, punctate pY816 immunoreactivity (G; arrows) within the shaft. Merged pY816 and GFP is shown in (I). Scale bar = 10 μm.

Supplementary Figure 5: (magenta-green version of Figure 9. pY816 TrkB immunoreactivity is enhanced within dendritic spines in CA1 SR following KA-SE, observed preferentially in the hippocampus ipsilateral to infusion.) A-I) Confocal micrographs from CA1 SR from a Thy1-GFP mouse treated with KA. Three *z*-sections are shown taken at 750 nm increments above (A-C; top), within (D-F; middle), and below (G-I; bottom) two GFP+ spines (E; arrows) of an apical dendrite that contain small pY816 puncta (D; arrows). Other spines (E; arrow with asterisk) do not appear to contain pY816 (D; arrow with asterisk). Note colocalization of pY816 with spines in the *z*-plane (observe panels from top to bottom and note arrows), such that these pY816 puncta are observable within the spine but not above or below it. Merged pY816 and GFP images are shown in (C, F, I). Scale bar = 2.5 μm. J) Quantification of percentages of GFP+ spines found to contain pY816 immunoreactivity in Thy1 GFP-

expressing mice in CA1 SR, CA1 SO, CA1 SLM, CA3 SR, the outer two-thirds of SML, and the outer two-thirds of IML. This was quantified under both NS (n=5) and KA (n=5) conditions, both ipsilateral (IPSI) and contralateral (CONTRA) to the side of infusion. In spines of CA1 SR ipsilateral to KA infusion, a 2.0-fold increase in the numbers of pY816+ spines was observed compared to NS treated animals ($p<0.01$, one-way ANOVA; $p<0.01$, *post-hoc* Bonferroni's test). The contralateral side demonstrated a more modest, 1.6-fold increase which was not significant. Data is from 994 spines analyzed under NS conditions, 1020 spines analyzed under KA conditions. No significant differences in the numbers of pY816+ spines were found in any of the other regions analyzed (CA1 SO $p=0.993$, 2097 spines; CA1 SLM $p=0.272$, 2428 spines; CA3 SR $p=0.899$, 2263 spines; SML $p=0.604$, 1940 spines; IML $p=0.128$, 1958 spines, one-way ANOVA). Quantification is presented as mean % of neuronal processes ± SEM; all data analyzed by one-way ANOVA and *post-hoc* Bonferroni's test; $^{**}p<0.01$.